Magnetic resonance spectroscopy and methionine positron emission tomography analysis for patients with lower-grade astrocytoma with marked invasiveness

Hirohito Yano (hirohito@herb.ocn.ne.jp)
Chubu Neurorehabilitation Hospital

Yuka Ikegame
Chubu Neurorehabilitation Hospital

Kazuhiro Miwa
Central Japan International Medical Center

Etsuko Owashi
Chubu Neurorehabilitation Hospital

Noriyuki Nakayama
Gifu University Graduate School of Medicine

Takashi Maruyama
Tokyo Women's Medical University

Kengo Matsunaga
Central Japan International Medical Center

Naoyuki Ohe
Gifu University Graduate School of Medicine

Hiroaki Takei
Central Japan International Medical Center

Souko Ikuta
Tokyo Women's Medical University

Tetsuya Yamada
Gifu University Graduate School of Medicine

Kazufumi Ohmura
Chubu Neurorehabilitation Hospital

Kazutoshi Yokoyama
Central Japan International Medical Center

Yoshihiro Muragaki
Tokyo Women's Medical University

Toru Iwama
Gifu University Graduate School of Medicine

Jun Shinoda
Chubu Neurorehabilitation Hospital

Research Article

Keywords: astrocytoma, MRI, MRS, methionine, PET, isocitrate dehydrogenase

Posted Date: May 25th, 2022

DOI: https://doi.org/10.21203/rs.3.rs-1643519/v1

Abstract

Background

The isocitrate dehydrogenase (IDH) status of patients with World Health Organization grade II or III astrocytoma is essential for understanding its biological features and determining therapeutic strategies. This study aimed to use radiological analysis to predict the IDH status of patients with lower-grade astrocytomas.

Methods

Forty-seven patients with grade II (17 cases) or III astrocytomas (30 cases), based on the 2016 World Health Organization Classification, underwent methionine (MET) positron emission tomography (PET) and magnetic resonance spectroscopy (MRS) on the same day between January 2013 and June 2020. The patients were retrospectively assessed. Immunohistochemistry showed 23 cases of IDH-mutant and 24 of IDH-wildtype. Based on FLAIR/T2 imaging, three doctors blinded to clinical data independently allocated 18 patients to the clear boundary group between the tumor and the normal brain and 29 to the unclear boundary group. The peak ratios of N-acetylaspartate (NAA) / creatine (Cr), choline (Cho) / Cr, and Cho/NAA and the tumor-to-normal region (T/N) ratio for maximum accumulation in MET PET were calculated. For statistical analysis, Fisher's exact test was used to assess associations between two variables, and the Mann–Whitney U test to compare the values between the IDH-wildtype and IDH-mutant groups. The optimal cut-off values of MET T/N ratio and MRS parameters for discriminating IDH-wildtype from IDH mutant were obtained using receiver operating characteristics curves.

Results

The unclear boundary group had significantly more IDH-wildtype cases than the clear boundary group (P < .001). The IDH-wildtype group had significantly lower Cho/Cr (< 1.84) and Cho/NAA (< 1.62) ratios (P = .02 and P = .047, respectively) and a higher MET T/N ratio (> 1.44, P = .02) than the IDH-mutant group. The odds for the IDH-wildtype were 0.22 for patients who fulfilled none of the four criteria, including boundary status and three ratios, and 0.9 for all four criteria.

Conclusions

These results suggest that the combination of MRI, MRS, and MET PET examination could be helpful for the prediction of IDH status in World Health Organization grade II/III gliomas.

Introduction

Since the 2016 World Health Organization (WHO; Geneva, Switzerland) classification of tumors incorporated molecular diagnosis, the patients' isocitrate dehydrogenase (IDH) status has been clinically important. For astrocytoma, the median survival of IDH-mutant (mut) and IDH wildtype (wt) are 9.3 years and 1.9 years, respectively.[1] One study[2] reported that IDH-mut WHO grade II astrocytomas showed sharp borders on T2-weighted imaging. In contrast, IDH-wt WHO grade II gliomas have a greater tumor volume and an infiltrative pattern on MR images,[3] and they are predominantly located in a single lobe with less contrast enhancement.[4] Park et al.[5] reported four imaging characteristics of IDH-wt tumors: nonlobar location, the proportion of enhancing tumor of > 33%, multifocal/multicentric distribution, and poor definition of nonenhancing margins. Therefore, it is assumed that gliomas showing aggressive behavior on magnetic resonance imaging (MRI) may be IDH-wt.

Immunohistochemistry and sequence tests are the gold standards for examining IDH status. However, the detection of 2-hydroxyglutarate in magnetic resonance spectroscopy (MRS) has shown a 90% or higher sensitivity and specificity for the prediction of IDH-mut.[6] This test is noninvasive, but it requires special software such as LCModel (L.A. Systems, Inc., Tokyo, Japan). In contrast, magnetic resonance spectroscopy (MRS) using standard markers such as choline (Cho), creatine (Cr), and N-acethylaspartate (NAA) is universally used and highly versatile in community hospitals. However, only one published study has sought to determine IDH status by using standard MRS for gliomas to the best of our knowledge.[7] Methionine (MET) positron emission tomography (PET) studies have shown significantly higher accumulation of MET in IDH-wt gliomas than in IDH-mut gliomas.[7–10]

This study investigated the relationships between MRI findings of tumor boundaries, standard MRS parameters, MET uptake ratio, and IDH status and discussed them pathologically.

Methods

Study population

We retrospectively enrolled 75 patients who underwent MET PET and MRS on the same day at our institution between January 2013 and June 2020. All patients had known pathological diagnoses of grade II or III astrocytomas, based on the 2016 WHO classification.[11] Three neurosurgeons (EO, YI, and KM) independently assessed the patterns observed via fluid-attenuated inversion recovery (FLAIR) or T2-weighted image (WI) imaging to differentiate the group with a clear boundary between the tumor and the normal brain and the group with an unclear boundary. At the time of imaging assessment, the reviewers established three categories for classifying tumors: clear boundary, unclear boundary, or neither. Assessments were based solely on imaging, as physicians were blinded to clinical data such as patient name, age, sex, and histological diagnosis.

From this initial cohort of 75 patients, we sought to analyze only the outcomes of patients for whom all three reviewers or two of the three reviewers could agree on tumor classification. The physicians' independent assessments aligned in 44 of the 75 (58.7%) cases studied. Specifically, their assessments

aligned as follows: 14 patients were classified as being in the clear boundary group, and 30 patients were classified as being in the unclear boundary group. In 10 (13.3%) cases, two of the three physicians agreed on classification, and the remaining physician was unable to decide; of these ten patients, the clinicians classified seven patients as being in the clear boundary group and three patients as being in the unclear boundary group. From this cohort of 54 patients, we further excluded seven patients with an unknown IDH status; thus, 47 cases (24 men, 23 women; average age = 47.0 years; age range = 19–89 years) were ultimately included in our analysis,

Of these 47 cases, we noted 17 cases of grade II astrocytoma and 30 cases of grade III astrocytoma, 23 cases of IDH-mut and 24 cases of IDH-wt (Table 1). There were 18 patients in the clear boundary group and 29 patients in the unclear boundary group (Table 1). The average age was significantly higher for the IDH-wt group than the IDH-mut group ($P = .005$) (Table 1). No significant differences existed in sex and WHO grade between the IDH status groups; however, the IDH status and MRI findings for boundary status were significantly different ($P < .001$; Table 1).

[Table 1]

PET

PET was conducted prior to MRI. Eminence STARGATE (Shimadzu Corporation, Kyoto, Japan) was used, which was equipped with a three-dimensional acquisition system (Shimadzu Corporation) that provided 99 transaxial images at 2.65 mm intervals. The in-plane spatial resolution (full width at half-maximum) was 4.8 mm, and the scans were conducted in three-dimensional mode. MET was injected intravenously at 3.5 MBq/kg through the cubital vein.

During PET data acquisition, head position was corrected using laser beams projected onto ink marks drawn on the forehead, and images were reconstructed using an ordered subset expectation-maximization algorithm. Tracer accumulation in the region of interest (ROI) was analyzed using the standard uptake value (SUV), defined as the activity concentration in the ROI at a fixed time point divided by the injected dose and then normalized to the patient's weight. The tumor-to-normal region (T/N) ratio of MET was calculated by dividing the maximum SUV of the tumor by the mean SUV of the contralateral normal frontal cortex. The ROI for the maximum tumor SUV was selected based on the areas with the highest tracer accumulation. The maximum tumor SUV was used instead of the mean SUV for the tumor to minimize the effect of tumor heterogeneity. Because of high and unexplained intersubjective SUV variability, we used the T/N ratio instead of the absolute SUV.

Coregistration of PET and MRI was conducted using the Dr. View image analysis software package (AJS, Tokyo, Japan). In this study, fusion images of PET and MRI are referred to as MET PET.

MRI

We used the Achieva 3.0T TX QD MRI system (Philips, Amsterdam, Netherlands) for transaxial T1-WI (repetition time (TR), 2200 ms; inversion time (TI), 950 ms; echo time (TE), 9.5 ms; field of view (FOV), 230

×230 $mm^{2;}$ matrix, 512×512); T2-WI (TR, 4000 ms; TE, 90 ms; FOV, 230×230 mm^2; matrix, 512×512); and FLAIR imaging (TR, 8000 ms; TI, 2400 ms; TE,120 ms; FOV, 230×230 mm^2; matrix, 512×512). The slice thickness was 5 mm with a 1-mm slice gap. A gadolinium-based contrast agent, gadoteridol (Eizai, Japan), was injected intravenously at 0.1 mL/kg body weight for contrast-enhanced studies.

To quantify the extent of the lesion, we measured the area of the hyperintense lesion on the FLAIR images and the area of the entire brain in the same cross-section by using ImageJ software (U.S. National Institutes of Health, Bethesda, MD, USA). We considered the area ratio as the spreading tumor ratio. For the T2/FLAIR image used for the reviewers' assessment, we selected the same slice as the cross-section showing the highest accumulation of MET in the tumor on MET PET.

MRS

Proton MRS was conducted simultaneously with conventional MRI using the single-voxel point-resolved spectroscopy technique with a TR of 2000 ms and TE of 288 ms. The total acquisition time required to obtain these parameters, including scanner adjustments, was <5 minutes. A cubic voxel with a side length of 2.0 cm was manually placed on the lesion, for which MET PET showed the highest accumulation. Spectra were generated using an internal scanner software, thereby providing automatic peak assignment and ratio calculations. The NAA/ Cr, Cho/Cr, and Cho/NAA peak ratios were recorded. Cr was used as the benchmark.

Pathological evaluation

We prepared formalin-fixed paraffin-embedded sections of labeled tissue for histology. The specimens underwent H&E staining and immunohistochemistry to determine IDH status using an anti-IDH1R132H monoclonal antibody (1:20; Dianova; Hamburg, Germany 1:20). Immunoreaction was considered positive when the tumor cells showed strong and diffuse staining for IDH1R132H.

The specimens were also stained with an anti-Ki-67 antibody (1:100; Dako, Tokyo, Japan) to evaluate tumor proliferation. The Ki-67 labeling index was visually quantified by counting the number of immunopositive nuclei in areas with the highest Ki-67 immunoreactivity as the percentage of Ki-67 positive cells per 1000 tumor cells.

The antigen was retrieved in an autoclave (121°C for 15 min). We used the Envision kit (Dako) as a source of secondary antibodies and 3,3-diaminobenzidine as the chromogen.

Statistical analysis

We used Fisher's exact test to assess associations between IDH status and sex, WHO grade, and tumor-brain boundary status, and the Mann–Whitney *U* test to compare the spreading tumor ratio, MRS parameters, MET T/N ratio, and Ki-67 labeling index between IDH-wt and IDH-mut groups.

Statistical significance was set at $P<.05$. Receiver operating characteristic (ROC) analysis was conducted to determine the optimal thresholds of the Cho/Cr, Cho/NAA, and MET T/N ratios for discriminating IDH-wt from IDH mut and the area under the curve. We determined the optimal sensitivity and specificity from the highest sum of the ROC curve. R software (R Project for Statistical Computing, Vienna, Austria, version 4.0.3) was used for all statistical analyses.

Results

The spreading tumor ratios were significantly higher for the unclear boundary group than for the clear boundary group (21.2 ± 12.5 vs. 6.6 ± 3.2, $P< .001$), but the correlation between boundary status and tumor grade was not significant ($P= .99$). Therefore, this finding confirmed that our reviewers' imaging-based classifications of the clear and unclear boundary groups were objectively different. Spreading tumor ratios were significantly higher for the IDH-wt group (20.7 ± 14.0) than for the IDH-mut group (11.1 ± 8.4) ($P= .008$) (Table 1). The association between tumor grade and IDH status was not significant ($P = .55$). By contrast, the association between boundary status and the IDH status was significant ($P < .001$); the unclear boundary group contained significantly more IDH-wt cases, whereas the clear boundary group contained significantly more IDH-mut cases (Table 1).

The Cho/Cr, Cho/NAA, and MET T/N ratios for the IDH-wt and IDH-mut groups showed significant differences ($P= .02$, $P= .047$, and $P= .02$, respectively); however, the NAA/Cr ratio and Ki-67 labeling index showed no significant difference between the two groups (Table 2). All MRS parameters and the Ki-67 labeling index showed no significant differences between the unclear and clear boundary groups. Only the MET T/N ratio was significantly different between the two groups (Table 2).

[Table 2]

We conducted ROC curve analyses to discriminate IDH-wt from IDH-mut based on the Cho/Cr, Cho/NAA, and MET T/N ratios, which showed significant differences between IDH-wt and IDH-mt statuses. The cut-off value for the Cho/Cr ratio was 1.84, with sensitivity and specificity of 82.6% and 62.5%, respectively. The cut-off value for the Cho/NAA ratio was 1.62, with sensitivity and specificity of 82.6% and 50.0%, respectively. The cut-off value for the MET T/N ratio was 1.44, with sensitivity and specificity of 91.7% and 52.2%, respectively. The area under the curve for the Cho/Cr, Cho/NAA, and MET T/N ratios was 0.70, 0.67, and 0.70, respectively (Fig. 1).

We then calculated the predictive accuracy for IDH-wt from the combination of the following four items: "unclear boundary," "Cho/Cr ratio ≤ 1.84," "Cho/NAA ratio ≤ 1.62," and "MET T/N ratio ≥ 1.44". The accuracies for predicting IDH-wt for the conditions of (1) no match, (2) one match, (3) two matches, (4) three matches, and (5) matches for all four items were 22.2%, 0%, 40.0%, 87.5%, and 90.0%, respectively (Fig. 2).

Representative cases

Case 1

A 19-year-old man presented with convulsions. MRI revealed a brain tumor in the right frontal lobe, which showed low signal intensity on T1WI and high signal intensity with clear boundaries on T2WI (Fig. 3A) and FLAIR imaging (Fig. 3B). The lesion showed no contrast enhancement. The spreading tumor ratio was 5.3%. MRS showed NAA/Cr, Cho/Cr, and Cho/NAA ratios of 0.83, 2.32, and 2.80, respectively (Fig. 3C). The MET T/N ratio was 1.25 (Fig. 3D). H&E staining showed cell proliferation with nuclear atypia, but no strong endothelial proliferation or central necrosis was observed (Fig. 3E). The Ki-67 labeling index was 7%. While immunohistochemistry for IDH1R132H showed diffuse positive staining (Fig. 3F), fluorescence in situ hybridization analysis for the loss of heterozygosity of 1p and 19q revealed no co-deletion. These results led to a final histological diagnosis of anaplastic astrocytoma, IDH-mut. The patient returned to his social life without neurological deficits and showed no post-craniotomy recurrence during four years of follow-up.

Case 2

A 70-year-old woman experienced gait disturbance due to bilateral lower-limb weakness. MRI showed a nonenhanced tumor bilaterally spreading to the periventricular white matter with unclear boundaries (Figs. 3G and 3H). The spreading tumor ratio was 55.2%. The NAA/Cr, Cho/Cr, and Cho/NAA ratios were 1.28, 1.55, and 1.22, respectively (Fig. 3I). The MET T/N ratio was 1.99 (Fig. 3J). These findings led to gliomatosis cerebri as the preoperative clinical diagnosis. H&E staining showed scattered large ganglion cells and atypical glial cells, but the cell density was not high (Fig. 3K). While immunohistochemistry showed IDH1R132H-negativity (Fig. 3L), the Ki-67 labeling index was 6.5%. The final histological diagnosis was diffuse IDH-wt grade II/III astrocytoma with a gliomatosis cerebri pattern. In the present study, we treated this case as grade III. The patient received 40 Gy whole-brain irradiation with temozolomide. She required full assistance seven months after the biopsy due to quadriplegia and confusion.

Discussion

Several reports exist regarding the prediction of IDH-mut based on the detection of 2-hydroxyglutarate.[6, 12–18] In addition, in one report,[7] the IDH status was predicted by using the combination of MRS and MET PET. Our study aimed to establish a method for predicting the IDH status and determine the pathological implications of the MRS and MET PET findings for predicting IDH status by comparing the unclear and clear boundary groups using preoperative MRI findings. We did not have special software to detect 2-hydroxyglutarate based on MRS; therefore, we relied upon the standard and versatile MRS parameters Cho, Cr, and NAA.

This study revealed more IDH-wt lower-grade astrocytic gliomas in the unclear boundary group than in the clear boundary group. This finding was supported by the significantly higher spreading tumor ratio in the IDH-wt group than in the IDH-mut group. By contrast, Baldock et al.[19] analyzed the MRIs of 172 patients

with contrast-enhanced gliomas and found no significant difference in the dispersal index between the IDH-wt and IDH-mut groups. However, we observed significantly more cases of IDH-wt in the unclear boundary group, which had a significantly higher Ki-67 labeling index than in the clear boundary group. Clinicians accordingly should consider a tumor with an unclear boundary as invasive and aggressive.

Gliomatosis cerebri was excluded from the 2016 WHO classification because it comprises a genetically and epigenetically heterogeneous group of diffuse gliomas.[20] We encountered seven cases that met the criteria of the 2007 WHO classification,[21] which defined them as extensively infiltrative diffuse gliomas involving at least three cerebral lobes.[21] Gliomatosis cerebri has two radiographic subtypes: gliomatosis cerebri without a solid component (type 1; the classic subtype) and gliomatosis cerebri with a solid component (type II).[22, 23] IDH-mut has frequently been observed in type II, but rarely in type I.[22, 23] Among our seven cases, six cases were type I and the remaining case was type II, and all seven cases were IDH-wt. However, IDH-mut type I cases have also been reported[24]; therefore, IDH-wt is not necessarily specific to type I.

Histological findings of necrosis and microvascular proliferation are reportedly more frequent in gliomatosis celebri with IDH-wt than those with IDH-mut.[23] However, H&E findings cannot generally predict IDH status. Determining the mechanism of invasion depends on IDH status as follows: For IDH-mut cases, the expression of oncogenes such as the platelet-derived growth factor receptor was associated with glioma formation[25] and the migratory capacity of glioma cells.[26, 27] For IDH-wt cases, the receptor tyrosine kinase-phosphatidylinositol-3/serine-threonine protein kinase-mechanistic target of rapamycin pathway has been reported to promote invasion.[28] Notably, the six-transmembrane epithelial antigen of prostate 3 is significantly more expressed in IDH-wt tumors than in IDH-mut tumors and is involved in the invasiveness of gliomas.[29] Regardless of the IDH status, the tumors all have molecular mechanisms involved in infiltration.

In the present study of lower-grade astrocytoma with marked invasiveness, the Cho/Cr and Cho/NAA ratios were significantly lower for IDH-wt cases. In general, Cho is a metabolic marker of cell membrane density and integrity[30] and may be elevated because of increased membrane synthesis in rapidly dividing tumor cells.[31] A surprising finding was that the Cho/Cr ratio was significantly lower in the IDH-wt group, although the MET T/N ratio and Ki-67 labeling index were significantly higher for the IDH-wt group than for the IDH-mut group. This finding may be because of low cell density, as observed in the pathological findings of Case 2. These results for the Cho/Cr and MET T/N ratios were consistent with reports by Kebir et al.[7] and Zhou et al[8] .

NAA is an internal neuronal marker, and it parallels the relatively constant neuronal cell density.[32] One report[33] showed a tendency toward a higher NAA peak for grade II gliomas than high-grade glioma. The NAA density decreases with increasing glioma grading, and the Cho/NAA ratio is a sensitive method for detecting differences in tumor growth.[34] In our data, the NAA/Cr ratio showed no significant difference between the IDH-wt and IDH-mut groups. However, the Cho/NAA ratio was significantly different between

the two groups because the Cho/Cr ratio was significantly lower for the former than for the latter, and the NAA/Cr ratio was slightly higher for the former. Thus, we showed that the Cho/Cr and Cho/NAA ratios were significantly lower for the IDH-wt group than for the IDH-mut group. Clinicians should consider marked invasive glioma on preoperative MRI with these MRS findings as a case of IDH-wt.

The cut-off values for the Cho/Cr, Cho/NAA, and MET T/N ratios for differentiating IDH-wt from IDH-mut cases in the present series obtained by ROC analyses were 1.84, 1.62, and 144, respectively. However, these values were obtained from a limited series; therefore, care must be taken to ensure versatility and reproducibility. A higher diagnostic rate of IDH-wt was associated with meeting more of the following criteria: Cho/Cr ≤ 1.84, Cho/NAA ≤ 1.62, T/N ratio ≥ 1.44, and an unclear boundary (Fig. 2). Therefore, these items seem reasonable for predicting IDH status. Representative Case 2 was expected to be IDH-wt because all of the criteria mentioned above were met. We believed that the findings showing multiple ganglion-like cells with sparse cell density affected the decrease in Cho/NAA and Cho/Cr ratios in this particular case.

The WHO Classification of Tumors, 5th edition[35] was released in 2022. It classifies all IDH-wt adult gliomas as grade 4. However, none of the patients in this study could be classified according to this version because they did not undergo grade 4-confirming molecular testing such as telomerase reverse transcriptase promoter mutation, epidermal growth factor receptor amplification, and chromosome 7 gain/chromosome 10 loss.

Conclusion

A decrease in the Cho/Cr or Cho/NAA ratio in an intra-axial brain tumor with unclear boundaries suggests IDH-wt. The Cho/Cr ratio is likely to be underestimated because the tumor cell density is sparse in an IDH-wt tumor, owing to its high infiltration. However, we considered that the neuronal cells in the IDH-wt group had a lower Cho/NAA ratio than those in the IDH-mut group. Although our study does not correspond to the new WHO classification, 5th edition, the pathological infiltrative nature of IDH-wt could be supported by MRS and MET PET information. This diagnostic method of combining MRI, MRS, and MET PET helped predict the IDH status of lower-grade astrocytoma. We need to verify the prediction of IDH status by this method through a future prospective study.

Abbreviations List

Cho
choline
Cr
creatine
FOV
field of view
FLAIR

fluid-attenuated inversion recovery
IDH
isocitrate dehydrogenase
H&E
hematoxylin & eosin
mut
mutant
MET
methionine
MRI
magnetic resonance imaging
MRS
magnetic resonance spectroscopy
NAA
N-acetylaspartate
PET
positron emission tomography
ROC
Receiver operating characteristic
ROI
region of interest
SUV
standard uptake value
TE
echo time
TI
inversion time
T/N
tumor-to-normal region
TR
repetition time
WHO
World Health Organization
WI
weighted image
wt
wildtype

Declarations

Ethics approval and consent to participate

All procedures were conducted based on the 1964 Helsinki Declaration and later amendments or comparable ethical standards. Approval was granted by the Ethics Committee of Kizawa Memorial Hospital (Minokamo City, Japan; approval no. 2021-001), the predecessor of Central Japan International Medical Center (Minokamo City, Japan). The committee also allowed informed consent to be waived due to the study's retrospective design and instructed us to post an information disclosure document on our hospital website (http://chubu-ryougo.jp/news/news/oshirase_220126.pdf) for patients who wanted to opt-out.

Consent for publication

We obtained written informed consent for publication from the patient (case 1) or the patient's relatives (case 2) included in the representative cases.

Availability of data and materials

The datasets used and analyzed during the current study are available from the corresponding author on reasonable request.

Competing interests

All authors declare that they have no competing interests that might be perceived to influence the results andor discussion reported in this paper.

Funding

Any external funding did not support this study.

Author's contributions

Conceptualization, HY and JS; Data curation, NN, NO, SI, YI, TY, EO, KO, and KaM; Formal analysis, HY and KaM, Investigation, NO, HT, KeM and KY; Validation, HY, SI, YI and KaM; Writing-Original graft preparation, HY; Writing-review & editing, KaM, TM and JS; Project administration, KY; Supervision, YM and TI and JS. All authors read and approved the final manuscript.

Acknowledgments

We would like to thank the radiology staff of Chubu Medical Center for Prolonged Traumatic Brain Dysfunction (Minokamo, Japan) for their technical support. We would like to thank the staff members of the pathology departments of Tokyo Women's Medical University (Tokyo, Japan), Gifu University (Gifu City, Japan), and Kizawa Memorial Hospital (Minokamo City, Japan) for their histology and pathology expertise. We would like to thank Editage (www.editage.com) for English language editing.

Author's information

[1]Department of Neurosurgery and Chubu Medical Center for Prolonged Traumatic Brain Dysfunction, Chubu Neurorehabilitation Hospital, 630 Shimo-kobi, Kobi-cho, Minokamo 505-0034, Japan

[2]Department of Clinical Brain Science, Gifu University Graduate School of Medicine, 1-1 Yanagido, Gifu City 501-1194, Japan

[3]Department of Neurosurgery, Central Japan International Medical Center, 1-1 Kenkou-no-machi, Minokamo City 505-8510, Japan

[4]Department of Neurosurgery, Gifu University Graduate School of Medicine, 1-1 Yanagido, Gifu City 501-1194, Japan

[5]Department of Neurosurgery, Tokyo Women's Medical University, 8-1 Kawada-cho, Shinjuku-ku, Tokyo 162-8666, Japan

[6] Department of Pathology, Central Japan International Medical Center, 1-1 Kenkou-no-machi, Minokamo City 505-8510, Japan

References

1. Pekmezci M, Rice T, Molinaro AM, et al. Adult infiltrating gliomas with WHO 2016 integrated diagnosis: additional prognostic roles of ATRX and TERT. Acta Neuropathol. 2017;133:1001-16. https://doi.org/10.1007/s00401-017-1690-1
2. Xing Z, Yang X, She D, et al. Noninvasive Assessment of IDH Mutational Status in World Health Organization Grade II and III Astrocytomas Using DWI and DSC-PWI Combined with Conventional MR Imaging. AJNR Am J Neuroradiol. 2017; 38:1138-44. http://doi.org/10.3174/ajnr.A5171
3. Metellus P, Coulibaly B, Colin C, et al. Absence of IDH mutation identifies a novel radiologic and molecular subtype of WHO grade II gliomas with dismal prognosis. Acta Neuropathol. 2010;120:719-29. http://doi.org/10.1007/s00401-010-0777-8
4. Qi S, Yu L, Li H, et al. Isocitrate dehydrogenase mutation is associated with tumor location and magnetic resonance imaging characteristics in astrocytic neoplasms. Oncol Lett. 2014;7:1895-1902. http://doi.org/10.3892/ol.2014.2013
5. Park YW, Han K, Ahn SS, et al. Prediction of IDH1-Mutation and 1p/19q-Codeletion Status Using Preoperative MR Imaging Phenotypes in Lower Grade Gliomas. AJNR Am J Neuroradiol. 2018;39:37-42. http://doi.org/10.3174/ajnr.A5421
6. Suh CH, Kim HS, Jung SC, et al. 2-Hydroxyglutarate MR spectroscopy for prediction of isocitrate dehydrogenase mutant glioma: a systemic review and meta-analysis using individual patient data. Neuro Oncol. 2018;20:1573-83. http://doi.org/10.1093/neuonc/noy113
7. Kebir S, Lazaridis L, Weber M, et al. Comparison of L-Methyl-11C-Methionine PET With Magnetic Resonance Spectroscopy in Detecting Newly Diagnosed Glioma. Clin Nucl Med. 2019;44:e375-e381.

http://doi.org/10.1097/RLU.0000000000002577

8. Zhou, W, Zhou, Z, Wen, J, et al. A Nomogram Modeling 11C-MET PET/CT and Clinical Features in Glioma Helps Predict IDH Mutation. Frontiers in oncology 2020;10:1200. https://doi.org/10.3389/fonc.2020.01200
9. Takei H, Shinoda J, Ikuta S, et al. Usefulness of positron emission tomography for differentiating gliomas according to the 2016 World Health Organization classification of tumors of the central nervous system. J Neurosurg 2019;16:1-10. https://doi.org/10.3171/2019.5.JNS19780
10. Nakajo K, Uda T, Kawashima T, et al. Diagnostic Performance of [11C]Methionine Positron Emission Tomography in Newly Diagnosed and Untreated Glioma Based on the Revised World Health Organization 2016 Classification. World Neurosurg. 2021;148:e471-e481. https://doi.org/10.1016/j.wneu.2021.01.012
11. Louis DN, Ohgaki H, Wiestler OD, et al: WHO Classification of Tumours of the Central Nervous System, revised ed 4. Lyon, International Agency for research on Cancer, 2016:16-27
12. Choi C, Ganji SK, DeBerardinis RJ, et al. 2-hydroxyglutarate Detection by magnetic resonance spectroscopy in IDH-mutated patients with gliomas. Nat Med. 2012;18:624–29. http://doi.org/10.1038/nm.2682
13. Pope WB, Prins RM, Albert Thomas M, et al. Noninvasive Detection of 2-hydroxyglutarate and other metabolites in IDH1 mutant glioma patients using magnetic resonance spectroscopy. J Neurooncol. 2012;107:197–205. http://doi.org/10.1007/s11060-011-0737-8
14. Natsumeda M, Igarashi H, Nomura T, et al. Accumulation of 2-hydroxyglutarate in gliomas correlates with survival: a study by 3.0-tesla magnetic resonance spectroscopy. Acta Neuropathol Commun. 2014;2:158. http://doi.org/10.1186/s40478-014-0158-y
15. Choi C, Raisanen JM, Ganji SK, et al. Prospective longitudinal analysis of 2-hydroxyglutarate magnetic resonance spectroscopy identifies broad clinical utility for the management of patients with IDH-mutant glioma. J Clin Oncol. 2016;34:4030–39. https://doi.org/10.1200/JCO.2016.67.1222
16. Nagashima H, Tanaka K, Sasayama T, et al. Diagnostic value of glutamate with 2-hydroxyglutarate in magnetic resonance spectroscopy for IDH1 mutant glioma. Neuro Oncol. 2016;18:1559–68. http://doi.org/10.1093/neuonc/now090
17. Tietze A, Choi C, Mickey B, et al. Noninvasive assessment of isocitrate dehydrogenase mutation status in cerebral gliomas by magnetic resonance spectroscopy in a clinical setting. J Neurosurg. 2018;128:391–8. http://doi.org/10.3171/2016.10.JNS161793
18. Bumes E, Wirtz FP, Fellner C, et al. Noninvasive prediction of IDH mutation in patients with glioma WHO II/III/IV based on F-18-FET PET-guided in vivo 1H-magnetic resonance spectroscopy and machine learning. Cancers (Basel). 2020;12:3406. http://doi.org/10.3390/cancers12113406
19. Baldock AL, Yagle K, Born DE, et al. Invasion and proliferation kinetics in enhancing gliomas predict IDH1 mutation status. Neuro Oncol. 2014;16(6):779-86. http://doi.org/10.1093/neuonc/nou027
20. Gielen GH, Simon M, Wiewrodt D, et al. Gliomatosis cerebri: no evidence for a separate brain tumor entity. Acta Neuropathol. 2016;131:309-19. http://doi.org/10.1007/s00401-015-1495-z

21. Fuller GN, Kros JM. Gliomatosis cerebri. 4th ed. In: Louis DN, Ohgaki H, Wiestler OD, et al, eds. WHO Classification of Tumour of the Central Nervous System. Lyon, France: International Agency for Research on Cancer, 2007:50-52
22. Chen S, Tanaka S, Giannini C, et al. Gliomatosis cerebri: clinical characteristics, management, and outcomes. J Neurooncol. 2013;112:267-75. http://doi.org/10.1007/s11060-013-1058-x
23. Seiz M, Tuettenberg J, Meyer J, et al. Detection of IDH1 mutations in gliomatosis cerebri, but only in tumors with additional solid component: evidence for molecular subtypes. Acta Neuropathol. 2010;120:261-7. http://doi.org/10.1007/s00401-010-0701-2
24. Narasimhaiah D, Miquel C, Verhamme E, et al. IDH1 mutation, a genetic alteration associated with adult gliomatosis cerebri. Neuropathology. 2012;32:30-7. http://doi.org/10.1111/j.1440-1789.2011.01216.x
25. Flavahan WA, Drier Y, Liau BB, et al. Insulator dysfunction and oncogene activation in IDH mutant gliomas. Nature. 2016;7:529:110-4. http://doi.org/10.1038/nature16490
26. Assanah M, Lochhead R, Ogden A, et al. Glial progenitors in adult white matter are driven to form malignant gliomas by platelet-derived growth factor-expressing retroviruses. J Neurosci. 2006;26:6781-90. http://doi.org/10.1523/JNEUROSCI.0514-06.2006
27. Masui K, Suzuki SO, Torisu R, et al . Glial progenitors in the brainstem give rise to malignant gliomas by platelet-derived growth factor stimulation. Glia. 2010;58:1050-65. http://doi.org/10.1002/glia.20986
28. Masui K, Kato Y, Sawada T, Mischel PS, Shibata N. Molecular and Genetic Determinants of Glioma Cell Invasion. Int J Mol Sci. 2017;18(12):2609. Published 2017 Dec 4. doi:10.3390/ijms18122609
29. Han M, Xu R, Wang S, et al. Six-Transmembrane Epithelial Antigen of Prostate 3 Predicts Poor Prognosis and Promotes Glioblastoma Growth and Invasion. Neoplasia 2018;20:543-4. http://doi.org/10.1016/j.neo.2018.04.002
30. Bulik M, Jancalek R, Vanicek J, et al. Potential of MR spectroscopy for assessment of glioma grading. Clin Neurol Neurosurg. 2013;115:146-53. http://doi.org/10.1016/j.clineuro.2012.11.002
31. Guo J, Yao C, Chen H, et al. The relationship between Cho/NAA and glioma metabolism: implementation for margin delineation of cerebral gliomas. Acta Neurochir (Wien). 2012;154:1361-70. http://doi.org/10.1007/s00701-012-1418-x
32. Pouwels PJ, Frahm J. Regional metabolite concentrations in human brain as determined by quantitative localized proton MRS. Magn Reson Med. 1998;39:53-60. http://doi.org/10.1002/mrm.1910390110
33. Nafe R, Herminghaus S, Raab P, et al. Preoperative proton-MR spectroscopy of gliomas–correlation with quantitative nuclear morphology in surgical specimen. J Neurooncol. 2003;63:233-45. http://doi.org/10.1023/a:1024249232454
34. Möller-Hartmann W, Herminghaus S, Krings T, et al. Clinical application of proton magnetic resonance spectroscopy in the diagnosis of intracranial mass lesions. Neuroradiology. 2002;44:371-81. http://doi.org/10.1007/s00234-001-0760-0

35. The WHO Classification of Tumouors Editorial Board, eds. WHO Classification of Tumours, 5th ed. Central Nervous System Tumours. Lyon: International Agency for research on Cancer; 2022

Tables

Table 1 and 2 are available in the Supplementary Files section.

Figures

Figure 1

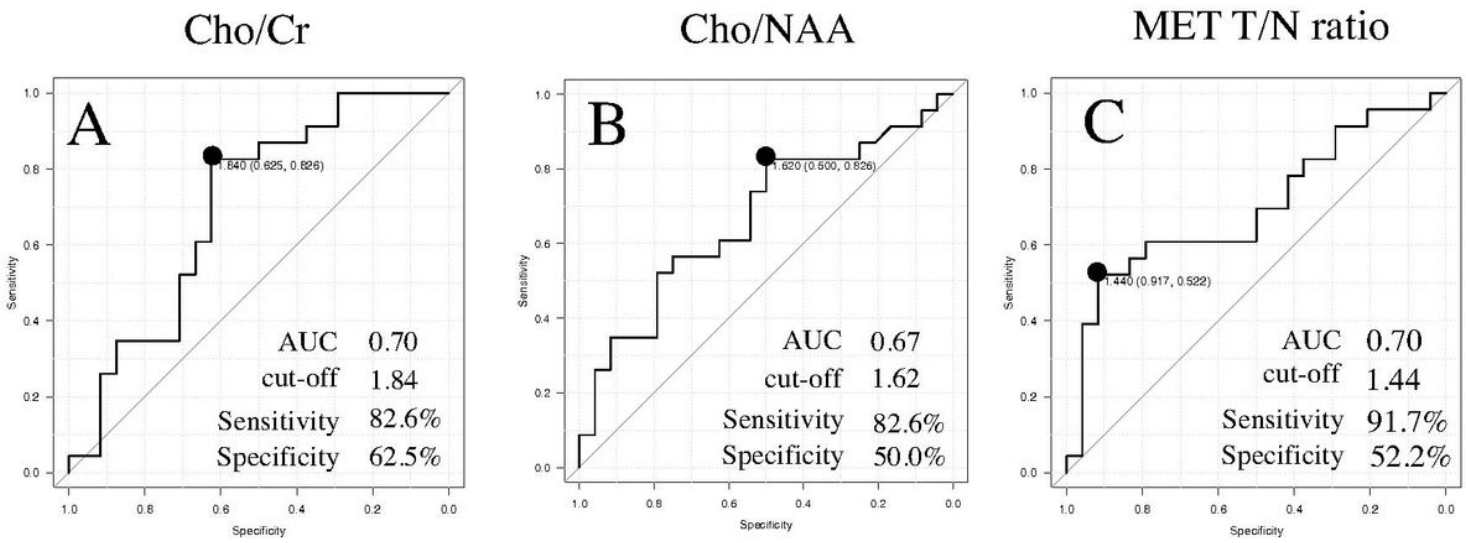

Figure 1

The ROC curves for the ratios of (A) Cho/Cr, (B) Cho/NAA, and (C) MET T/N for differentiating IDH-wt from IDH-mut cases. The area under the curve, cut-off, sensitivity, and specificity values are shown for each ratio. The closed circle indicates the point where the sum of the sensitivity and specificity is at its maximum.

MET = methionine; T/N = tumor-to-normal region; IDH = isocitrate dehydrogenase; wt = wildtype; mut = mutant; AUC=area under the curve

Figure 2

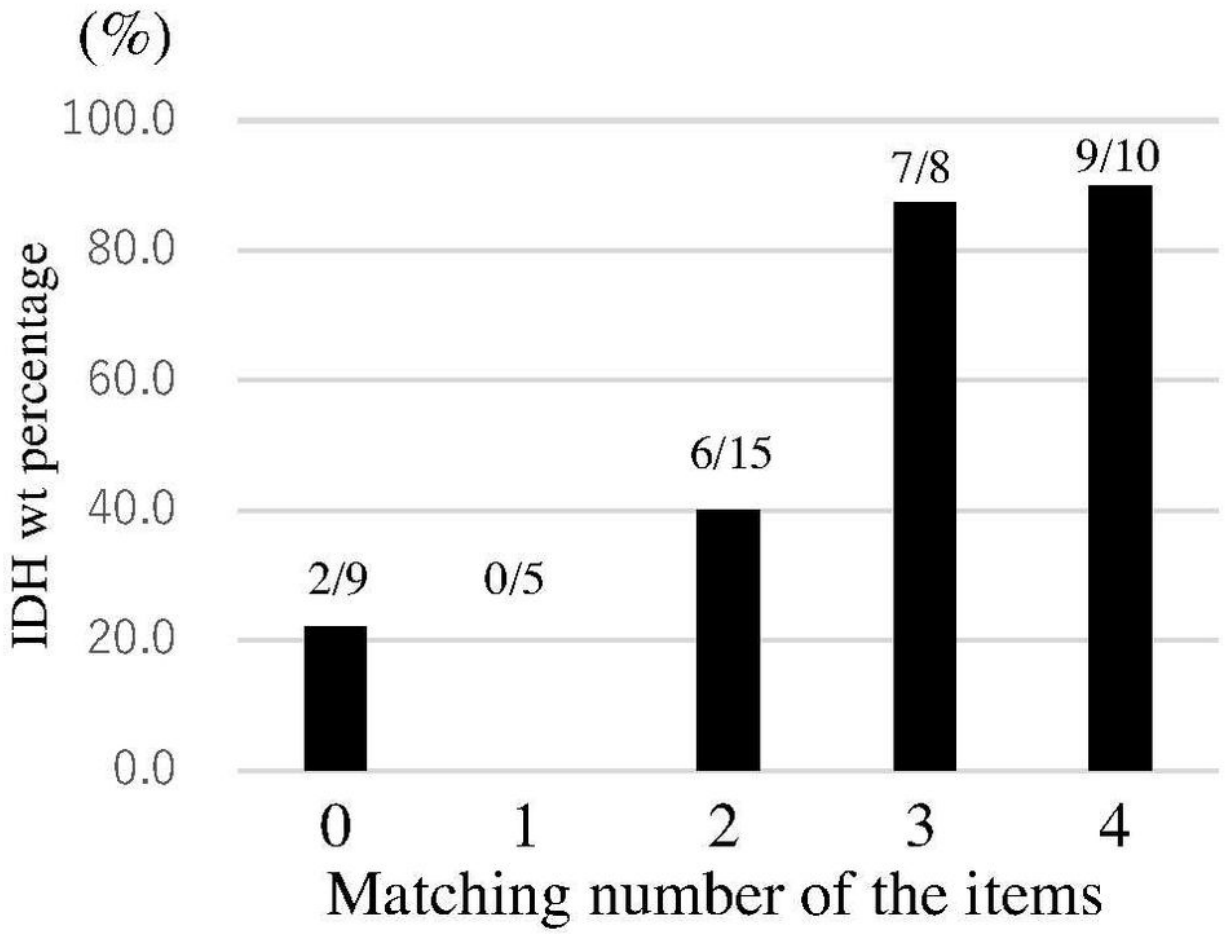

Figure 2

The bar graph shows the predictive rate of IDH-wt for combinations of the following criteria: Cho/Cr ≤1.84, Cho/NAA ≤1.62, T/N ratio ≥1.44, and unclear boundary. The figure in the bar indicates the number of IDH-wt cases per number of cases diagnosed, based on each of the criteria.

IDH = isocitrate dehydrogenase; wt = wildtype; mut = mutant

Figure 3

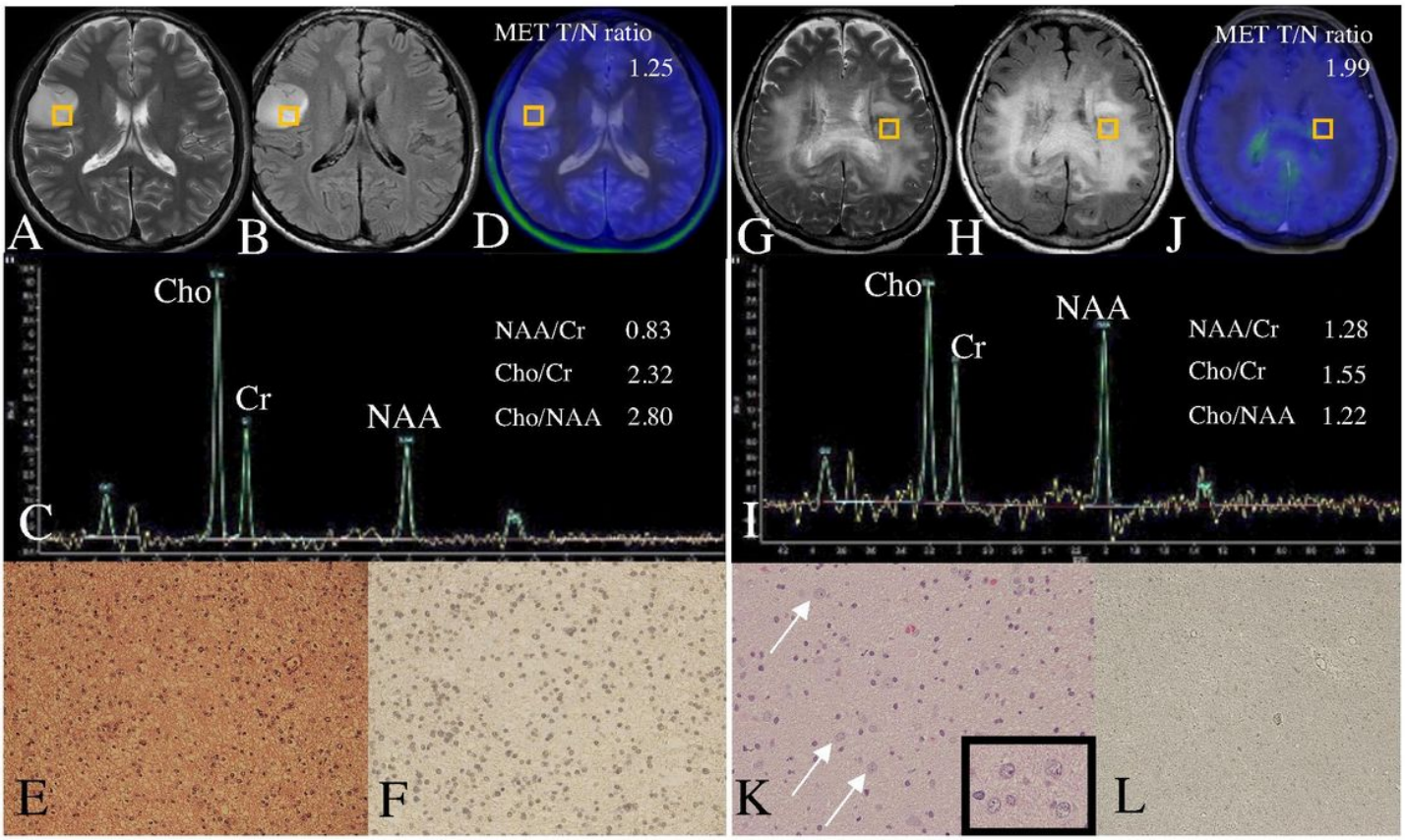

Figure 3

(A–F) Representative Case 1. (G–L) Representative Case 2. (A and G) T2WI images. (B and H) FLAIR images. (C and I) MRS findings. (D and J) MET PET images. The yellow boxes in these images indicate the ROI for MRS. (E and K) Findings with H&E staining. (F and L) Immunohistochemistry for IDH1R132H shows (F) immune-positivity (i.e., IDH-mut) and (L) immune-negativity (i.e., IDH-wt). The arrows and the inset in K show ganglion-like cells. The NAA/Cr, Cho/Cr, Cho/NAA, and MET T/N ratios are shown for each representative case. The original magnifications are ×100 for E, F, K, and L and ×200 for the inset in K.

MET = methionine; IDH = isocitrate dehydrogenase; wt = wildtype; mut = mutant; T/N = tumor-to-normal region

Supplementary Files

This is a list of supplementary files associated with this preprint. Click to download.

- Table1.xlsx
- Table2.xlsx